

Generative adversarial learning with optimal input dimension and its adaptive generator architecture

Zhiyao Tan*, Ling Zhou* and Huazhen Lin^{†‡}

New Cornerstone Science Laboratory,
Center of Statistical Research and School of Statistics,
Southwestern University of Finance and Economics, Chengdu, China

Abstract

In this paper, we investigate the impact of the input dimension on the generalization error in generative adversarial networks (GANs). In particular, we first provide both theoretical and practical evidence to validate the existence of an optimal input dimension (OID) that minimizes the generalization error. Then, to identify the OID, we introduce a novel framework called generalized GANs (G-GANs), which includes existing GANs as a special case. By incorporating the group penalty and the architecture penalty developed in the paper, the proposed G-GANs have several intriguing features. First, our framework offers adaptive dimensionality reduction from the initial dimension to a dimension necessary for generating the target distribution. Second, this reduction in dimensionality also shrinks the required size of the generator network architecture, which is automatically identified by the proposed architecture penalty. Both reductions in dimensionality and the generator network significantly improve the stability and the accuracy of the estimation and prediction. Theoretical support for the consistent selection of the input dimension and the generator network is provided. Third, the proposed algorithm involves an end-to-end training process, and the algorithm allows for dynamic adjustments between the input dimension and the generator network during training, further enhancing the overall performance of the G-GANs. Extensive experiments conducted with simulated and benchmark data demonstrate the superior performance of the proposed G-GANs. In particular, compared to that of off-the-shelf methods, the proposed method achieves an average improvement of 45.68% in the CT slice dataset, 43.22% in the MNIST dataset and 46.94% in the FashionMNIST dataset in terms of the maximum mean discrepancy or Fréchet inception distance. Moreover, the features generated based on the input dimensions identified by G-GANs align with visually significant features: thickness and angle of inclination of the digits in MNIST and fabric quantity and clothing style in FashionMNIST.

Keywords: GANs; Optimal input dimension; Adaptive generator architecture.

*Co-first authors.

[†]Corresponding author. Email address: linhz@swufe.edu.cn.

[‡]The research was supported by National Key R&D Program of China (No.2022YFA1003702), National Natural Science Foundation of China (Nos. 11931014 and 12271441), and New Cornerstone Science Foundation.

1 Introduction

Deep generative models, such as generative adversarial networks (GANs), have gained significant attention in recent years due to their ability to learn complex data distributions and to generate high-quality samples (Goodfellow et al., 2014; Radford et al., 2016; Arjovsky et al., 2017; Karras et al., 2019). GANs are performed by training a discriminator f and a generator g in a confrontational fashion until the samples are generated by an easy-to-sample source distribution ν are indistinguishable from the sampling of the target distribution μ . Particularly, GANs are formulated as a minimax optimization problem at the population level:

$$g^* = \arg \min_{g \in \mathcal{G}} \max_{f \in \mathcal{F}} \mathcal{L}(f, g), \quad (1)$$

$$\mathcal{L}(f, g) = \mathbb{E}_{x \sim \mu}[f(x)] - \mathbb{E}_{z \sim \nu}[f(g(z))], \quad (2)$$

where both the generator and the discriminator classes, denoted as \mathcal{G} and \mathcal{F} , respectively, are parameterized by neural networks.

The underlying principle of GANs is built upon the assumption that real-world datasets possess low-dimensional intrinsic structures (Arjovsky and Bottou, 2017; Dahal et al., 2022). Leveraging this assumption, GANs create high-dimensional data of dimension D from low-dimensional input variables z with a significantly smaller dimension of d , i.e., $d \ll D$. However, both the theoretical and practical understanding of d remain unclear. In particular, given observed data and an easy-to-sample distribution, such as a uniform or Gaussian distribution, how the generalization error of a GAN depends on the input dimension d .

The generalization error of GANs can be decomposed into three main components: the generator approximation error, the discriminator approximation error, and the statistical error. The generator approximation error pertains to the capacity of neural networks to approximate the target distribution. Lee et al. (2017) shows that the target distributions composed of Barron functions (Barron, 1993) can be approximated by a neural network. However, when the target distribution is

Gaussian, [Bailey and Telgarsky \(2018\)](#) shows that the generator approximation error takes the form $\mathcal{O}(W)^{-\mathcal{O}(L/D)}$, where W and L represent the width and depth of the neural network, respectively. To relax the restriction of a Gaussian target distribution to any continuous density, [Lu and Lu \(2020\)](#) establish a generator approximation rate $\mathcal{O}(W^{-\frac{1}{D}})$ of neural networks with the requirement that $L = \mathcal{O}(\log W)$, and the same dimension for the source and the target distributions, d is taken to be D . This rate is further extended to target distributions with Hölder densities by [Chen et al. \(2020a\)](#). However, all these works suffer from the curse of dimensionality due to the approximation rates $\mathcal{O}(W)^{-\mathcal{O}(L/D)}$ or $\mathcal{O}(W^{-\frac{1}{D}})$ for medium to large D . Recent studies ([Perekrestenko et al., 2020](#); [Yang et al., 2022](#); [Huang et al., 2022](#)) demonstrate that a high-dimensional target distribution can be generated by one-dimensional distributions, and the approximation error vanishes as L becomes infinite or $W \geq 7D + 1$. These methods focus on approximating the empirical distribution, and the regularity or smoothness of the target distribution is ignored, which may lead to poor generalization errors. This scenario is illustrated in [Figure 1](#) and supplementary [Figure E2](#). In [Figure 1](#), the leftmost side of each graph shows the generalization errors for $d = 1$, which are much larger than those for $d > 1$. In supplementary [Figure E2](#), on the GRID dataset, the samples generated by WGAN-GP ([Gulrajani et al., 2017](#)) with $d = 2$ perform much better than those with $d = 1$ due to the former capture spatial information.

The discriminator approximation error relies on the ability of the neural network to represent functional classes of D -dimensional data because the discriminator works on the observed data. Recent advances in deep learning have spurred numerous studies on quantifying the approximation error of deep ReLU networks based on the number of parameters or neurons, and the results have already been used to bound the discriminator approximation error ([Huang et al., 2022](#); [Chen et al., 2020a](#); [Yarotsky, 2017, 2018](#); [Shen, 2020](#); [Jiao et al., 2023](#)), which has order $\mathcal{O}((WL)^{-2\beta/D})$, where β is the smoothness index of the evaluation function class.

Regarding the statistical error, [Chen et al. \(2020a\)](#) demonstrated that it scales as $\mathcal{O}(n^{-\frac{\beta}{2\beta+D}})$

when \mathcal{F} belongs to a Hölder class with smoothness index β or has a low-dimensional linear structure. The distance induced by the Hölder class is quite general. However, these results still suffer the curse of dimensionality. When D is large, challenges arise in explaining the performance of GANs. In [Schreuder et al. \(2021\)](#) and [Dahal et al. \(2022\)](#), the authors demonstrate that the statistical error converges at a rate of $\mathcal{O}(\max(n^{-\frac{\beta}{d^*}}, n^{-\frac{1}{2}}))$ if we take $d = d^*$, where d^* is the intrinsic dimension. Since prior knowledge of the intrinsic dimension is usually unavailable in practice, [Block et al. \(2022\)](#) and [Huang et al. \(2022\)](#) further establish the rate without the restriction of $d = d^*$, which is a significant contribution to the field.

Based on existing research on the above three components, we can see that the input dimension d and the intrinsic dimension d^* play crucial roles in the generator approximation error and the statistical error of GANs, respectively. Given that d^* is inherently unchangeable, several interesting questions can be raised: Can we choose a proper input dimension to minimize generalization errors? How does the generalization error of GANs vary with the input dimension? Additionally, what network architecture should the generator g have for a given input dimension? [Figure 1](#) illustrates how the generalization error of GANs first decreases then increases with the growth of the input dimension and the corresponding generator architecture while keeping the discriminator network constant. This elucidates the presence of the optimal input dimension for GANs and indicates the need to design and to train GANs with the optimal input dimension and the corresponding generator architecture that minimizes the generalization error. In this paper, we provide new theoretical and methodological insights into input dimensions, and we bridge the gap between the generalization error of GANs and the input dimension to answer the questions above.

Our key strategy to address these problems is to incorporate a matrix \mathbf{B} into GANs. In particular, we generalize GANs by considering the following framework:

$$\mathcal{L}(f, g, \mathbf{B}) = \mathbb{E}_{x \sim \mu}[f(x)] - \mathbb{E}_{z \sim \nu}[f(g(\mathbf{B}z))], \quad (3)$$

Obviously, when \mathbf{B} is the identity matrix, the criterion $\mathcal{L}(f, g, \mathbf{B})$ is reduced to $\mathcal{L}(f, g)$, as defined in (2). Hence, the existing GANs can be regarded as a special case of the generalized GANs (G-GANs) in (3). The introduction of \mathbf{B} offers us an opportunity to identify the input dimension through distinguishing rows $\mathbf{B} = (B_1, \dots, B_d)'$ as zero or nonzero. By excluding all the B_j that are zero, we can determine the number of nonzero elements in the vector $\mathbf{B}z$, which, in turn, determines the input dimension. Hence, the proposed G-GANs offer adaptive dimensionality reduction from the initial z dimension to a dimension necessary to generate the target distribution.

In addition to imposing the group sparsity penalty (Yuan and Lin, 2006) into \mathbf{B} , we incorporate a designed architecture penalty into the generator g , as shown later in Section 3. In this way, we present a powerful and adaptive estimation for the input dimension and the corresponding generator network architecture, leading to enhanced accuracy and stability in estimation and prediction, as illustrated in Figure 1. Unlike traditional two-step methods that first estimate the intrinsic dimension and then design the network accordingly (Schreuder et al., 2021), the proposed procedure is implemented through an end-to-end training process, and this procedure allows for dynamic adjustments between the input dimension and the generator network architecture during training, further enhancing the overall performance of the G-GANs. Comprehensive experiments on various simulated datasets, the CT slice dataset and two benchmark image datasets, MNIST and FashionMNIST, demonstrate the superior effectiveness of our approach. In particular, in comparison to the off-the-shelf models, we achieved an average improvement of 45.68% in the CT slice dataset, 43.22% in the MNIST dataset and 46.94% in the FashionMNIST dataset in terms of the maximum mean discrepancy (MMD) or Fréchet inception distance (FID); see Tables 2 to 4. Moreover, as illustrated in Figure 4 and supplementary Figure E3, the generated features based on the input dimensions identified by G-GANs align with visually significant features. For example, they represent the thickness and the angle of inclination of digits in MNIST and the fabric quantity and clothing style in FashionMNIST, implying a degree of interpretability in these input dimensions.

In addition to the superior practical performance as mentioned above, this work is the first attempt to explicitly show the effect of the input dimension d on the generalization error of GANs, particularly regarding generator approximation error, as shown in Theorem 2.1. This approach is significantly different from existing works that assume either $d = D$ or $d = 1$. For the former case, i.e., $d = D$, the established approximation rate of $\mathcal{O}(W)^{-\mathcal{O}(L/D)}$ or $\mathcal{O}(W^{-\frac{1}{D}})$ (Bailey and Telgarsky, 2018; Lu and Lu, 2020) produces the curse of dimensionality, especially for large D . For the latter case, i.e., $d = 1$, the generator approximation error is overlooked due to the vanishing approximation error for the empirical target distribution. As mentioned above, approximating the empirical distribution instead of the population distribution can lead to overfitting and can result in poor generalization error, as depicted in Figure 1 and supplementary Figure E2. In contrast to these studies exclusively focusing on either $d = D$ or $d = 1$, our derived Theorem 2.1 shows how the generator approximation error and the statistical error rely on the input dimension d and the size of the generated sample m . Particularly, when $m > n$, the generator approximation error and the statistical error are characterized by $\mathcal{O}_p(n^{\frac{-\beta_1}{2\beta_1+d}} + \inf_{\bar{g}^d \in \mathcal{H}^{\beta_1}([0,1]^d)} d_{\mathcal{F}}(\bar{g}_{\#}^d \nu^d, g_{0\#}^{d_0} \nu^{d_0}))$ and $\mathcal{O}_p(n^{\frac{-\beta_1}{2\beta_1+d}} \log^2 n + n^{\frac{-\beta_2}{2\beta_2+d^*}} \log^2 n)$, respectively, where d_0 is the minimal input dimension (MID) defined in Definition 2.2 and β_1 and β_2 are the smoothness indices of the Hölder class for the generator and the discriminator functions, respectively. $d_{\mathcal{F}}(\cdot, \cdot)$ is defined by (5). If $d < d_0$, the term $n^{\frac{-\beta_1}{2\beta_1+d}}$ is well controlled, while the term $\inf_{\bar{g}^d \in \mathcal{H}^{\beta_1}([0,1]^d)} d_{\mathcal{F}}(\bar{g}_{\#}^d \nu^d, g_{0\#}^{d_0} \nu^{d_0})$ remains significantly different from zero because of the limitation of approximating a d_0 -dimensional Hölder function by using a smaller d -dimensional counterpart. When $d \geq d_0$, the generator approximation error $\inf_{\bar{g}^d \in \mathcal{H}^{\beta_1}([0,1]^d)} d_{\mathcal{F}}(\bar{g}_{\#}^d \nu^d, g_{0\#}^{d_0} \nu^{d_0})$ vanishes. However, as the input dimension d increases, a larger generator network becomes necessary, leading to an increase in the statistical error. Consequently, there exists a trade-off between the generator approximation error and the statistical error, suggesting the existence of an optimal input dimension d . This is consistent with the practical performance shown in Figure 1.

In addition, we note that in most existing works, it is assumed that m can be arbitrarily large

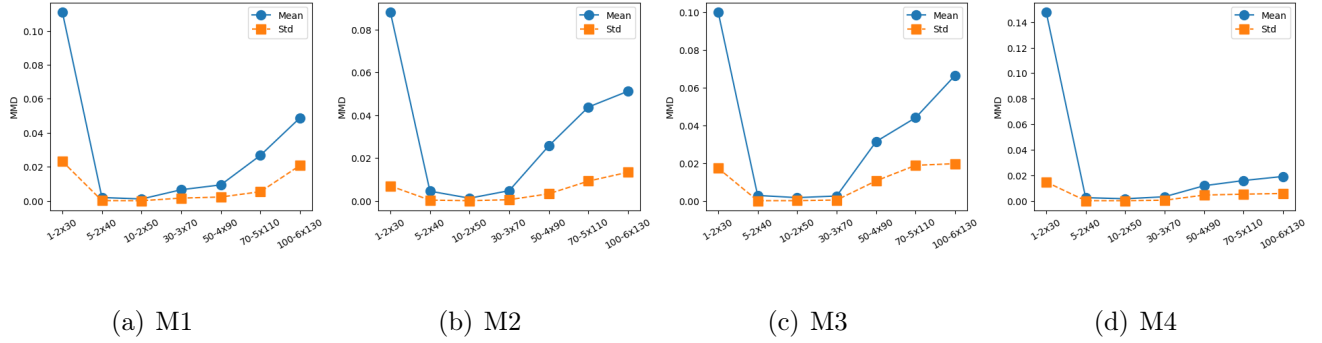


Figure 1: The mean (blue solid line) and standard deviation (Std, orange dotted line) of Maximum Mean Discrepancy (MMD) of SNGANs (Miyato et al., 2018) based on 10 replications with varying input dimensions and corresponding generator architectures, where $d-l \times w$ indicates the generator with the input dimension d , depth l and width w . (M1)-(M4) refer to four numerical simulations, described in detail in Section 5.

so that the statistical error induced by m can be ignored (Arora et al., 2017; Zhang et al., 2018; Schreuder et al., 2021; Block et al., 2022; Dahal et al., 2022). Only a few authors explicitly show the impact of m . For $d = D$, Chen et al. (2020a) shows that when $m \geq n$, the impact of m can be ignored, and the generalization error is determined by $\mathcal{O}(n^{-\frac{2\beta}{2\beta+D}})$. Huang et al. (2022) shows that for $d = 1$, only when $m \geq n^{2+2\beta/D} \log^6 n$ can the impact of m be ignored. However, in practice, given that n is already large, such an extraordinarily large requirement on m is practically infeasible due to limited storage and time costs. Based on our Theorem 2.1, a well-selected d , compact generator architecture, and $m \geq n$ are sufficient to yield superior performance in approximating the population target distribution. Thus, we further develop a novel adaptive method to automatically determine the optimal d and its corresponding generator architecture. Theoretical support for the consistency of the input dimension and the generator architecture is provided in Theorem 3.1.

The remainder of this paper is organized as follows. We begin by introducing the preliminaries and notation. In Section 2, we establish a theory to uncover a trade-off between the approximation error of the generator and the statistical error. We introduce the proposed G-GANs method, and we establish the theoretical properties of the estimators, including the consistency of the input dimension and the generator architecture, in Section 3. The implementation procedure is presented

in Section 4. In Section 5, we conduct extensive simulation studies and apply our method to the CT slice dataset and two benchmark image datasets, MNIST and FashionMNIST. Finally, we conclude our findings in Section 6. We provide additional numerical experiment results and proofs in the supplementary material.

2 Theoretical results

In this paper, we consider a feedforward neural network (FNN) with a ReLU activation function to approximate the generator and the discriminator functions. In particular, a ReLU neural network with L hidden layers is a collection of mappings $\phi : \mathbb{R}^{N_0} \rightarrow \mathbb{R}^{N_{L+1}}$ of the form $\phi(x) = T_L \circ \sigma \circ T_{L-1} \circ \dots \circ \sigma \circ T_0(x)$, where $\phi_1 \circ \phi_2(x) := \phi_1(\phi_2(x))$ represents the composition of two functions ϕ_1 and ϕ_2 . $\sigma(x) := \max(x, 0)$ is the ReLU function, which is applied elementwise; $T_l(x) := A_l x + c_l$ is an affine transformation with $A_l \in \mathbb{R}^{N_{l+1} \times N_l}$ and $c_l \in \mathbb{R}^{N_{l+1}}$ for $l = 0, 1, \dots, L$, and N_l is the number of neurons in layer l . We term $W = \max\{N_1, N_2, \dots, N_L\}$ and L the *width* and the *depth*, respectively, of the neural network. The *size* \mathcal{S} is defined as the total number of parameters in the network ϕ , i.e., $\mathcal{S} = \sum_{i=0}^L N_{i+1} \times (N_i + 1)$. We denote by $\mathcal{NN}(W, L, \mathcal{S}, \mathcal{B})$ the set of ReLU neural networks ϕ with width W , depth L , size \mathcal{S} and $\|\phi\|_\infty \leq \mathcal{B}$ for some $0 < \mathcal{B} < \infty$, where $\|\phi\|_\infty$ is the supnorm of the function ϕ .

We consider the Hölder class as the evaluation class \mathcal{H} to which the true functions belong. Let $\beta = s + r > 0$, $r \in (0, 1]$ and $s = \lfloor \beta \rfloor$, where $\lfloor \beta \rfloor$ denotes the largest integer strictly smaller than β . The Hölder class $\mathcal{H}^\beta(\mathcal{X})$ takes the form $\mathcal{H}^\beta(\mathcal{X}) := \{h : \mathcal{X} \rightarrow \mathbb{R}, \max_{\|\alpha\|_1 < s} \|\partial^\alpha h\|_\infty \leq 1, \max_{\|\alpha\|_1 = s} \sup_{x \neq y} \frac{|\partial^\alpha h(x) - \partial^\alpha h(y)|}{\|x - y\|_2^r} \leq 1\}$, where $\partial^\alpha = \partial^{\alpha_1} \dots \partial^{\alpha_d}$ with $\alpha = (\alpha_1, \dots, \alpha_d)^\top$, $\|\alpha\|_1 = \sum_{i=1}^d \alpha_i$ and $\|\alpha\|_2 = \sqrt{\sum_{i=1}^d \alpha_i^2}$. The Hölder class is broad enough to cover most applications. However, the evaluation class \mathcal{H} does not have to coincide with the generator class \mathcal{G} or the discriminator class \mathcal{F} , which consist of ReLU-based FNNs. For a measurable mapping ν , we define the push-forward

measure $g_{\#}\nu$ as $g_{\#}\nu(\mathcal{A}) := \nu(g^{-1}(\mathcal{A}))$ for a measurable set \mathcal{A} .

Based on a finite collection of samples $X_1, \dots, X_n \stackrel{i.i.d.}{\sim} \mu$ and $Z_1, \dots, Z_m \stackrel{i.i.d.}{\sim} \nu$, we replace μ and ν with their empirical counterparts $\mu_n = \frac{1}{n} \sum_{i=1}^n \delta_{X_i}$ and $\nu_m = \frac{1}{m} \sum_{j=1}^m \delta_{Z_j}$, respectively, and we estimate g by

$$\hat{g} = \arg \min_{g \in \mathcal{G}} \max_{f \in \mathcal{F}} \hat{\mathcal{L}}(f, g) := \arg \min_{g \in \mathcal{G}} \max_{f \in \mathcal{F}} \left\{ \frac{1}{n} \sum_{i=1}^n f(X_i) - \frac{1}{m} \sum_{j=1}^m (f(g(Z_j))) \right\}. \quad (4)$$

We first investigate the generalization error of the GANs defined in (4). This error is evaluated by the integral probability metric (IPM) (Müller, 1997) between the target distribution μ and the learned distribution $\hat{g}_{\#}\nu$ with respect to the evaluation class \mathcal{H} , which has the form of

$$d_{\mathcal{H}}(\hat{g}_{\#}\nu, \mu) = \max_{h \in \mathcal{H}} \mathbb{E}_{x \sim \mu}[h(x)] - \mathbb{E}_{z \sim \nu}[h(\hat{g}(z))]. \quad (5)$$

By choosing different \mathcal{H} s, IPM can express many commonly used metrics (Arjovsky et al., 2017; Dziugaite et al., 2015; Mroueh et al., 2018).

Let the inequality $A \preceq B$ represent $A \leq CB$ for a positive constant C , $A \wedge B = \min(A, B)$, and $\Phi_1 \circ \Phi_2 := \{\phi_1 \circ \phi_2 : \phi_1 \in \Phi_1, \phi_2 \in \Phi_2\}$ represents the composition of two function classes Φ_1 and Φ_2 . We denote the support set of μ as Ω . In existing works (Chen et al., 2020a; Huang et al., 2022), an upper bound on the risk \hat{g} has been obtained in terms of the evaluation class \mathcal{H} , which is decomposed into the following three terms (Lemma 9 in Huang et al. (2022)):

$$d_{\mathcal{H}}(\hat{g}_{\#}\nu, \mu) \preceq \mathcal{E}(\mathcal{H}, \mathcal{F}, \Omega) + \inf_{g \in \mathcal{G}} d_{\mathcal{H}}(g_{\#}\nu, \mu_n) + \{d_{\mathcal{H}}(\mu, \mu_n) \wedge d_{\mathcal{F}}(\mu, \mu_n) + d_{\mathcal{F} \circ \mathcal{G}}(\nu, \nu_m)\}, \quad (6)$$

where $\mathcal{E}(\mathcal{H}, \mathcal{F}, \Omega) := \sup_{h \in \mathcal{H}} \inf_{f \in \mathcal{F}} \|h - f\|_{\infty}$ is the discriminator approximation error from \mathcal{F} to \mathcal{H} on Ω , which quantifies the discrepancy between the function classes \mathcal{F} and \mathcal{H} . The second term $\inf_{g \in \mathcal{G}} d_{\mathcal{H}}(g_{\#}\nu, \mu_n)$ represents the generator approximation error, which measures how well the empirical distribution μ_n can be approximated by ν through the transformation $g \in \mathcal{G}$ with respect to the metric $d_{\mathcal{H}}$. The third term represents the statistical error, which accounts for the differences between the empirical distributions μ_n and ν_m and their population counterparts. Notably, the upper bound

in the decomposition (6) is not sufficiently tight to allow us to discern the impact of \hat{g} . This occurs because, in the derivation, the use of the inequality $d_{\mathcal{H}}(\hat{g}_{\#}\nu_m, \mu_n) \leq d_{\mathcal{H}}(g_{\#}^*\nu_m, \mu_n)$ leads to the omission of the term associated with \hat{g} . To accurately calibrate the impact of learning g , we derive a new decomposition via an explicit expression of \hat{g} in the third term. That is,

Proposition 2.1. *Let us assume \mathcal{F} is symmetric, i.e., $\phi \in \mathcal{F}$ holds if and only if $-\phi \in \mathcal{F}$. Let g^* and \hat{g} be the population and the empirical GAN estimators (1) and (4), respectively. Then, for any evaluation class \mathcal{H} , it holds that*

$$d_{\mathcal{H}}(\hat{g}_{\#}\nu, \mu) \preceq \mathcal{E}(\mathcal{H}, \mathcal{F}, \Omega) + d_{\mathcal{H}}(g_{\#}^*\nu, \mu) + \{d_{\mathcal{F}}(\hat{g}_{\#}\nu, \mu) - d_{\mathcal{F}}(g_{\#}^*\nu, \mu)\}. \quad (7)$$

The proof of Proposition 2.1 is straightforward by simple decomposition, and detailed proofs can be found in the Supplementary Materials B. A similar decomposition to that of (7) can be found in Zhou et al. (2023) for the conditional sampling problem. The decompositions in equations (6) and (7) differ in two ways. First, in terms of the generator approximation error in the second terms of both (6) and (7), we shift our attention from approximating the empirical distribution μ_n to approximating the population distribution μ , ensuring sufficient generative capability within \mathcal{G} . Second, the statistical error in the third term of (7) accounts for the discrepancy between the performance of the estimator \hat{g} and the optimal possible estimator in \mathcal{G} , while the statistic error in the third term of (6) accounts for only the differences between the empirical distributions and their population versions.

In addition to Proposition 2.1, we need two definitions to express the generalization error of GANs. Following Schreuder et al. (2021), we assume that the true source distribution ν has been accessed and that there is a real generation function behind the target distribution. Let us denote the true generator function g_0 , which is supported on a bounded set; for simplicity, we assume this bounded set to be $[0, 1]^d$. Without loss of generality, we assume $\Omega \subseteq [0, 1]^D$. Since the true function may not be unique, we define:

Definition 2.1. A mapping class $\mathcal{G}_0 := \bigcup_{d \leq D} \{g_0 : [0, 1]^d \rightarrow [0, 1]^D, g_0 \in \mathcal{H}^{\beta_1}([0, 1]^d)\}$ such that $\forall g_0 \in \mathcal{G}_0, \mu = g_{0\#}(\nu)$.

Definition 2.1 implies that $\min_{g \in \mathcal{G}_0} \max_{h \in \mathcal{H}} \mathcal{L}(h, g) \equiv \min_{g \in \mathcal{G}_0} \max_{f \in \mathcal{F}} \mathcal{L}(f, g)$ since $\mu \equiv g_{0\#}(\nu)$ leads to $f \circ \mu \equiv f \circ g_{0\#}(\nu)$ regardless of whether f belongs to \mathcal{F} or \mathcal{H} . Because there may be multiple different ds that can generate the target distribution μ , we give the following definition for the minimal input dimension.

Definition 2.2 (Minimal input dimension). We write g^d as the d -dimensional function and ν^d as the source distribution of the d -dimension. The minimal input dimension (MID) is defined as

$$d_0 := \min_d \{d \mid \mu = g_{0\#}^d(\nu^d), g_0 \in \mathcal{G}_0\},$$

where the minimum is taken among all ds such that (g^d, ν^d) can exactly generate the target distribution.

We now use Theorem 2.1 to explicitly show the upper bound of the generalization error in terms of the sample size and the neural network architectures. Without confusing the context, we abbreviate g^d and ν^d as g and ν , respectively. Based on Proposition 2.1, the results of approximation errors (Huang et al., 2022; Jiao et al., 2023), the covering number on the neural network (Bartlett et al., 2019) and by using empirical process techniques, we obtain the following theorem.

Theorem 2.1. Suppose the target distribution $\mu = g_{0\#}(\nu)$, the true generators belong to $\mathcal{H}^{\beta_1}([0, 1]^d)$ and the evaluation class is $\mathcal{H} = \mathcal{H}^{\beta_2}([0, 1]^D)$ ($\beta_2 \geq 1$). Then there exists a generator class $\mathcal{G} = \{g : \mathbb{R}^d \rightarrow \mathbb{R}^D \mid g \in \mathcal{NN}(W_{\mathcal{G}}, L_{\mathcal{G}}, \mathcal{S}_{\mathcal{G}}, \mathcal{B}_{\mathcal{G}})\}$ with

$$W_{\mathcal{G}}L_{\mathcal{G}} \preceq n^{\frac{d}{2(2\beta_1+d)}}, \quad (8)$$

and a discriminator class $\mathcal{F} = \{f : \mathbb{R}^D \rightarrow \mathbb{R} \mid f \in \mathcal{NN}(W_{\mathcal{F}}, L_{\mathcal{F}}, \mathcal{S}_{\mathcal{F}}, \mathcal{B}_{\mathcal{F}})\}$ with

$$W_{\mathcal{F}}L_{\mathcal{F}} \preceq n^{\frac{D}{2(2\beta_2+D)}}, \quad (9)$$

so that GAN estimator (4) satisfies

$$\begin{aligned}
d_{\mathcal{H}^{\beta_2}}(\hat{g}_{\#}\nu, \mu) = & \mathcal{O}_p \left(n^{\frac{-\beta_2}{2\beta_2+D}} + \left\{ n^{\frac{-\beta_1}{2\beta_1+d}} + \inf_{\bar{g}^d \in \mathcal{H}^{\beta_1}([0,1]^d)} d_{\mathcal{F}}(\bar{g}_{\#}^d \nu^d, g_{0\#}^{d_0} \nu^{d_0}) \right\} \right. \\
& \left. + \left\{ n^{\frac{-\beta_1}{2\beta_1+d}} \log^2 n + n^{\frac{-\beta_2}{2\beta_2+D}} \log^2 n + m^{\frac{-1}{2}} n^{\frac{d}{2(2\beta_1+d)}} \log^{\frac{3}{2}} n \log^{\frac{1}{2}} m + m^{\frac{-1}{2}} n^{\frac{D}{2(2\beta_2+D)}} \log^{\frac{3}{2}} n \log^{\frac{1}{2}} m \right\} \right). \tag{10}
\end{aligned}$$

Based on Theorem 2.1, we can see that the discriminator approximation error is bounded by $\mathcal{O}_p(n^{\frac{-\beta_2}{2\beta_2+D}})$, the generator approximation error is $\mathcal{O}_p(n^{\frac{-\beta_1}{2\beta_1+d}} + \inf_{\bar{g}^d \in \mathcal{H}^{\beta_1}([0,1]^d)} d_{\mathcal{F}}(\bar{g}_{\#}^d \nu^d, g_{0\#}^{d_0} \nu^{d_0}))$, and the statistical error is $\mathcal{O}_p(n^{\frac{-\beta_1}{2\beta_1+d}} \log^2 n + n^{\frac{-\beta_2}{2\beta_2+D}} \log^2 n + m^{\frac{-1}{2}} n^{\frac{d}{2(2\beta_1+d)}} \log^{\frac{3}{2}} n \log^{\frac{1}{2}} m + m^{\frac{-1}{2}} n^{\frac{D}{2(2\beta_2+D)}} \log^{\frac{3}{2}} n \log^{\frac{1}{2}} m)$. The approximation error $\mathcal{O}_p(n^{\frac{-\beta_2}{2\beta_2+D}})$ and the statistical error $\mathcal{O}_p(n^{\frac{-\beta_2}{2\beta_2+D}} \log^2 n)$ from the discriminator imply that when the dimension of the observed data D is large, the process suffers from the curse of dimensionality. In recent studies (Nakada and Imaizumi, 2020; Huang et al., 2022; Block et al., 2022), the authors have highlighted an important insight: The intrinsic low dimensionality of observed data is the main factor that determines the performance of deep neural networks. This finding suggests that if there exists a constant C and an intrinsic dimension d^* ($d^* \leq D$) such that $N(\epsilon, \Omega, \|\cdot\|_{\infty}) \leq C\epsilon^{-d^*}$, the two terms $\mathcal{O}_p(n^{\frac{-\beta_2}{2\beta_2+D}})$ and $\mathcal{O}_p(n^{\frac{-\beta_2}{2\beta_2+D}} \log^2 n)$ can be improved to $\mathcal{O}_p(n^{\frac{-\beta_2}{2\beta_2+d^*}})$ and $\mathcal{O}_p(n^{\frac{-\beta_2}{2\beta_2+d^*}} \log^2 n)$, respectively, by choosing $W_{\mathcal{F}}L_{\mathcal{F}} \preceq n^{\frac{d^*}{2(2\beta_2+d^*)}}$, where $N(\epsilon, \Omega, \rho)$ is the covering number of Ω under the metric ρ with radius ϵ .

It is interesting to compare the error bound in expression (10) with the existing results, which either assume $d = D$ or $d = 1$. When $d = D$, our results with $\beta_1 = \beta_2 = \beta$ and $m > n$ simplify to $\mathcal{O}_p(n^{\frac{-\beta}{2\beta+D}} \log^2 n)$, which is consistent with the results in Chen et al. (2020a). When $d = 1$, Huang et al. (2022) uses a specific architecture that handles the generator approximation error attributed to the following three conditions. First, the generator size, $W_{\mathcal{G}}^2 L_{\mathcal{G}} \preceq n$, is much larger than that in our proposal, i.e., $W_{\mathcal{G}} L_{\mathcal{G}} \preceq n^{\frac{d}{2(2\beta_1+d)}}$. Second, their approach, based on memorizing empirical data, overlooks the smoothness of the target distribution, leading to poor generalizability. Finally, their theoretical requirement $m > n^{2+2\beta/d} \log^6 n$ (Theorem 5 in Huang et al. (2022)) is impractical. For instance, with $n = 10$ thousand, m must reach approximately 100 million, incurring intensive

economic and time costs. More aggressively, in most existing studies the authors assume that m can be arbitrarily large, which indicates that the generator is actually obtained via

$$\hat{g}_n = \arg \min_{g \in \mathcal{G}} \max_{f \in \mathcal{F}} \left(\frac{1}{n} \sum_{i=1}^n f(\mathbf{X}_i) - \mathbb{E}(f(g(\mathbf{Z}_j))) \right) := \arg \min_{g \in \mathcal{G}} \max_{f \in \mathcal{F}} \tilde{\mathcal{L}}(f, g).$$

In practice, for any realization m , we have two additional terms: the last two terms in equation (10) for the statistical errors of the generator and discriminator based on m generated samples. Clearly, as long as $m > n$, the last two terms are dominated by the former two terms $n^{\frac{-\beta_1}{2\beta_1+d}} \log^2 n + n^{\frac{-\beta_2}{2\beta_2+D}} \log^2 n$ in (10), indicating that the term induced by m samples can be ignored if $m > n$.

Theorem 2.1 implies that a well-selected d , compact architecture, and reasonable m can yield superior performance in approximating the population target distribution. Specifically, Theorem 2.1 suggests that the choice of the input dimension d can affect the convergence rate by influencing the generator approximation error and the statistical error. The generator approximation error first decreases then increases as the input dimension d increases. Particularly, when $d < d_0$, the first term $n^{\frac{-\beta_1}{2\beta_1+d}}$ is well controlled, while the second term $\inf_{\bar{g}^d \in \mathcal{H}^{\beta_1}([0,1]^d)} d_{\mathcal{F}}(\bar{g}_{\#}^d \nu^d, g_{0\#}^{d_0} \nu^{d_0})$ remains significantly distant from zero because of the limitation of approximating a d_0 -dimensional Hölder function by using a smaller d -dimensional counterpart. When $d \geq d_0$, the term $\inf_{\bar{g}^d \in \mathcal{H}^{\beta_1}([0,1]^d)} d_{\mathcal{F}}(\bar{g}_{\#}^d \nu^d, g_{0\#}^{d_0} \nu^{d_0})$ or the generator approximation error vanishes. However, as the input dimension d increases, according to the inequality (8), the width and depth of the required generator architecture increase: A larger generator network becomes necessary, leading to an increase in the statistical error. Consequently, there exists a trade-off between the generator approximation error and the statistical error, suggesting the existence of an optimal input dimension d . By choosing the optimal input dimension for d and its corresponding generator architecture, a faster convergence rate can be achieved for the GAN estimator. Based on Theorem 2.1, we can directly obtain the following corollary to characterize the optimal input dimension:

Corollary 2.1. *Under the conditions of Theorem 2.1, if $m > n$, the GAN estimator (4) achieves*

the optimal error rate with $d = d_0$ on the order of

$$d_{\mathcal{H}^{\beta_2}}(\hat{g}_{\#}\nu, \mu) = \mathcal{O}_p\left(n^{\frac{-\beta_2}{2\beta_2+D}} \log^2 n + n^{\frac{-\beta_1}{2\beta_1+d_0}} \log^2 n\right).$$

Hence, d_0 is the optimal input dimension (OID) that minimizes the generalization errors. In the next section, we develop a novel adaptive method for choosing d_0 and the generator architecture simultaneously.

3 Generalized GANs

As mentioned in Section 1, a key strategy for identifying the OID is to introduce an index matrix \mathbf{B} , leading to the generalized GANs (G-GANs) framework (3). Since the row of indices \mathbf{B} determines the input dimension, determining the OID is equivalent to identifying nonzero rows of \mathbf{B} , which can be automatically implemented by incorporating a group sparsity penalty on \mathbf{B} . Moreover, according to Theorem 2.1, the size and the architecture of the generator should be adaptively adjusted by the OID, which is implemented by removing redundant hidden layers, by reducing the width and by forcing the redundant parameters to 0. Here, we note that, as long as the product of the width and depth of the network architecture satisfies the inequality (8) in Theorem 2.1, the optimal rate is achievable. That is, we can either select a proper depth with a fixed width or change the width with a fixed depth. Since a shallow network with a large width often demands less optimization effort than does a deep network with a small width (Glorot and Bengio, 2010; Srivastava et al., 2015; He et al., 2016), we hence prespecify the width with a large constant. Then, we determine the generator architecture by appropriately selecting its depth. In practical deep neural network (DNN) implementations, the depth is usually given in advance, and changing the depth requires retraining a new network. This limitation hinders the dynamic adjustment between d and the corresponding depth of the generator architecture. To address this, we propose a new strategy based on the key observation that if layer l is redundant, the affine transformation $T_l(x) = A_l x + c_l$ is not necessary;

that is, the information from $T_l(x)$ equals that from x . As a result, A_l can be replaced by an identity matrix and $c_l = 0$, which is realized by imposing a depth penalty $\|A_l - \mathbf{I}\|_1 + \|c_l\|_1$, where \mathbf{I} is an identity matrix with the same dimensions as A_l .

Let us assume that the generative class \mathcal{G} is parameterized by a ReLU neural network $\mathcal{NN}(W_{\mathcal{G}}, L_{\mathcal{G}}, \mathcal{S}_{\mathcal{G}}, \mathcal{B}_{\mathcal{G}})$ with parameters $\theta := \{A_l, c_l\}_{l=0}^{L_{\mathcal{G}}}$ and that the discriminator class \mathcal{F} is parameterized by $\mathcal{NN}(W_{\mathcal{F}}, L_{\mathcal{F}}, \mathcal{S}_{\mathcal{F}}, \mathcal{B}_{\mathcal{F}})$ with parameters w . Denote $\mathcal{W}_{\mathbf{B}} = \{\mathbf{B} : \mathbf{B} \in \mathbb{R}^{d \times d}, \|\mathbf{B}\|_{\infty} \leq \kappa_{\mathcal{W}}\}$ with the i -th row of a matrix \mathbf{B} denoted by $\mathbf{B}^{[i,:]} = (\mathbf{B}^{[i,j]}, j = 1, \dots, d)^T$. Then, we consider the following objective for G-GANs:

$$\left(\hat{\mathbf{B}}, \hat{\theta}\right) = \arg \min_{\mathbf{B} \in \mathcal{W}_{\mathbf{B}}, \theta: g_{\theta} \in \mathcal{G}} \max_{w: f_w \in \mathcal{F}} \left\{ \frac{1}{n} \sum_{i=1}^n f_w(\mathbf{X}_i) - \frac{1}{m} \sum_{j=1}^m f_w(g_{\theta}(\mathbf{B}\mathbf{Z}_j)) + \mathcal{L}_{reg}(\mathbf{B}, \theta) \right\}, \quad (11)$$

where $\mathcal{L}_{reg}(\mathbf{B}, \theta) = \lambda_1 M(\mathbf{B}) + \lambda_2 P(\theta) + \lambda_3 Q(\theta)$, $M(\mathbf{B}) = \sum_i \|\mathbf{B}^{[i,:]}\|_2 = \sum_i \sqrt{\sum_j \mathbf{B}^{[i,j]^2}}$ is the group sparsity penalty on the \mathbf{B} th row, $P(\theta) = \sum_{l=1}^{L_{\mathcal{G}}-1} \|A_l - \mathbf{I}\|_1 + \|c_l\|_1$ and $Q(\theta) = \|\theta\|_1$ are the architecture penalties, including the depth and the sparsity penalties. λ_1 , λ_2 and λ_3 are hyperparameters. As λ_1 , λ_2 and λ_3 increase, the number of nonzero rows in \mathbf{B} , the depth of the generator architecture and the number of nonzero components in θ decrease, resulting in a lower input dimension and a simpler neural network architecture. Hence, the automatic selection of d and the generator architecture can be accomplished by tuning the parameters λ_1 , λ_2 and λ_3 ; see Section 4 for details. Let us denote the resulting estimators by \hat{d} and $\hat{\gamma} = (\hat{\mathbf{B}}, \hat{\theta})$ for the number of nonzero rows of $\hat{\mathbf{B}}$ and $\gamma = (\mathbf{B}, \theta)$, respectively.

Next, we theoretically demonstrate that G-GANs with the objective function (11) are capable of selecting the OID and the corresponding generator network in terms of selection consistency. The following notation is needed to establish the theory. Without loss of generality, we partition \mathbf{B} into two parts, $\mathbf{U} \in \mathbb{R}^{d_0 \times d}$ and $\mathbf{V} \in \mathbb{R}^{(d-d_0) \times d}$, i.e., $\mathbf{B} = [\mathbf{U}^{\top}, \mathbf{V}^{\top}]^{\top}$. Then, to demonstrate the consistency of the selection of the input dimension, show that $\|\hat{\mathbf{U}}^{[i,:]}\|_2 \neq 0$ for $i = 1, \dots, d_0$, and $\|\hat{\mathbf{V}}^{[j,:]}\|_2 = 0$ for $j = 1, \dots, d - d_0$ with probability 1. as $n, m \rightarrow \infty$. Since the depth and sparsity depend on the width, we denote $\Theta^*(W) = \{\theta^* : (\mathbf{B}^*, \theta^*) \in \arg \min_{\mathbf{B} \in \mathcal{W}_{\mathbf{B}}, \theta: g_{\theta} \in \mathcal{G}} \{d_{\mathcal{F}}(g_{\theta} \circ \mathbf{B}_{\#}\nu, \mu), \mathbf{B} =$

$[\mathbf{U}^\top, \mathbf{0}^\top]^\top, \mathbf{U} \in \mathbb{R}^{d_0 \times d}, A_l \in \mathbb{R}^{W \times W}, 1 \leq l \leq L_G\}$ for the parameters set of generator with the width W under the OID.

The minimal depth is then denoted by $l_\theta(W) = \min_{l^*} \{l^* : l^* = \text{dep}(\theta^*), \theta^* \in \Theta^*(W)\}$, where $\text{dep}(\theta^*)$ is the depth of θ^* . Hereafter, we drop W for notational simplicity without confusion. Then, the estimation of the generator achieves consistency in depth selection if $\mathbb{P}(\text{dep}(\hat{\theta}) = l_\theta) \rightarrow 1$ as $n, m \rightarrow \infty$. For the size of generator, we denote $n_\theta = \min_{\check{\theta}^* \in \check{\Theta}^*} \|\check{\theta}^*\|_0$ as the minimal size of the generator under the OID and minimal depth, where $\check{\Theta}^* = \{\check{\theta}^* : \text{dep}(\check{\theta}^*) = l_\theta, \check{\theta}^* \in \Theta^*\}$ is the parameter set of the generator under the OID and minimal depth. Notably, although $\check{\theta}^*$ satisfying $\|\check{\theta}^*\|_0 = n_\theta$ is not unique due to the unidentifiability of the neural network, n_θ is unique. Then, the size selection consistency for the generator network is established by showing that $\mathbb{P}(\|\hat{\theta}\|_0 = n_\theta) \rightarrow 1$, as $n, m \rightarrow \infty$. Overall, we denote the parameter set of neural networks with OID, minimal depth and minimal size by $\Gamma^* = \{\gamma^* = (\mathbf{B}^*, \theta^*) : (\mathbf{B}^*, \theta^*) \in \arg \min_{\mathbf{B} \in \mathcal{W}_B, \theta: g_\theta \in \mathcal{G}} \{d_{\mathcal{F}}(g_\theta \circ \mathbf{B}_\# \nu, \mu), \mathbf{B}^* = [\mathbf{U}^\top, \mathbf{0}^\top]^\top, \mathbf{U} \in \mathbb{R}^{d_0 \times d}, A_l \in \mathbb{R}^{W \times W}, 1 \leq l \leq L_G, \text{dep}(\theta^*) = l_\theta, \|\theta^*\|_0 = n_\theta\}\}$. Let $d(\hat{\gamma}, \Gamma^*) := \min_{\gamma^* \in \Gamma^*} \|\hat{\gamma} - \gamma^*\|_2$, and we need the following two assumptions to establish consistency in the selection.

Assumption 3.1. For any $\check{\theta}_1^*, \check{\theta}_2^* \in \check{\Theta}^*$, $\|\check{\theta}_1^*\|_1 \leq \|\check{\theta}_2^*\|_1$ implies $\|\check{\theta}_1^*\|_0 \leq \|\check{\theta}_2^*\|_0$.

Assumption 3.2. For any $\tilde{\theta}_1^*, \tilde{\theta}_2^* \in \tilde{\Theta}^*$, there exists a constant $M_b < \infty$ such that $\|\tilde{\theta}_1^* - \tilde{\theta}_2^*\|_2 \leq M_b$ where $\tilde{\Theta}^* = \{\tilde{\theta}^* : (\tilde{\mathbf{B}}^*, \tilde{\theta}^*) \in \arg \min_{\mathbf{B} \in \mathcal{W}_B, \theta: g_\theta \in \mathcal{G}} d_{\mathcal{F}}(g_\theta \circ \mathbf{B}_\# \nu, \mu)\}$.

Assumption 3.1 concerns the connection of the L_1 norm and the L_0 norm for the parameters within $\check{\Theta}^*$. Based on the four numerical simulation datasets outlined in Section 5, the empirical analysis presented in Supplementary Figure E1 illustrates a monotonic relationship between the L_1 norm and the L_0 norm, providing support for Assumption 3.1. This difference may be attributed to the relatively small magnitudes of all the neural network parameters (Bellido, 1993; Huang et al., 2021). Assumption 3.2 focuses on the bounded difference between any two parameters in $\tilde{\Theta}^*$. This assumption is a relaxation of the assumption that the L_1 norm of any parameter is bounded, a

condition frequently required in the neural network literature (Chen et al., 2020a).

Theorem 3.1. *Considering that the generator class $\mathcal{G} = \{g : \mathbb{R}^d \rightarrow \mathbb{R}^D \mid g \in \mathcal{NN}(W_G, L_G, \mathcal{S}_G, \mathcal{B}_G)\}$*

with

$$W_G L_G \preceq n^{\frac{d}{2(2\beta_1+d)}}, \quad (12)$$

and the discriminator $\mathcal{F} = \{f : \mathbb{R}^D \rightarrow \mathbb{R} \mid f \in \mathcal{NN}(W_F, L_F, \mathcal{S}_F, \mathcal{B}_F)\}$ with

$$W_F L_F \preceq n^{\frac{D}{2(2\beta_2+D)}}, \quad (13)$$

suppose that Assumptions 3.1 and 3.2 hold. Let $\hat{\gamma}$ be the estimator of (11), when $m > n$, if $\lambda_1 = o(1)$, $\lambda_2 = o(\lambda_1)$, $\lambda_3 = o(\lambda_2)$, $(n^{\frac{-\beta_1}{2\beta_1+d}} + n^{\frac{-\beta_2}{2\beta_2+D}}) \log^2 n = o(\lambda_3)$, we deduce that

$$d(\hat{\gamma}, \Gamma^*) = o_p(1). \quad (14)$$

The detailed proof of Theorem 3.1 can be found in Supplementary C. The entire proof includes four parts: convergence to the optimal parameter set, input dimension consistency, depth and size selection consistency for the generator, where the first is achieved by the Lojasiewicz inequality (Ji et al., 1992; Colding and Minicozzi, 2014) and Young’s inequality. The second is established by following a similar idea as those in Dinh and Ho (2020b,a), and the last two parts can be represented by the unidentifiability of the neural network, and the relationship between the L_1 penalty and L_0 penalty in $\check{\Theta}^*$ based on Assumption 3.1.

Theorem 3.1 shows that G-GANs can identify the OID and the corresponding generator architecture with appropriate choices of λ_1 , λ_2 and λ_3 . The conditions $\lambda_2 = o(\lambda_1)$ and $\lambda_3 = o(\lambda_1)$ are required because the generator architecture relies on the chosen input dimension. That is, we need to determine the input dimension before identifying the generator architecture. The condition $\lambda_3 = o(\lambda_2)$ implies that the depth should be identified before determining the sparse structure of the generator architecture. These conditions are natural for implementing our strategy for identifying the structure of the generator. The requirement that λ_1 , λ_2 and λ_3 exceed the statistical

error $(n^{\frac{-\beta_1}{2\beta_1+d}} + n^{\frac{-\beta_2}{2\beta_2+D}}) \log^2 n$ is to prevent cases where redundant dimensions or parameters fail to converge to 0 due to randomness.

4 Implementation

In this section, we present the detailed implementation of G-GANs. We adopt the mini-batch stochastic gradient descent method (Bottou, 2010; Kingma and Ba, 2015) to find the solution to (11). There are two technical issues in implementing the algorithm: the selection of appropriate penalty parameters and optimizing the neural network parameters with the L_1 penalty.

To mitigate bias stemming from penalties, we allow $\lambda_1, \lambda_2, \lambda_3$ to change as iteration continues. Particularly, we start with small penalty parameters, and we gradually increase them before subsequently decreasing them. The strategy is considered because the parameters or vectors are quite random in early iterations and then become stable as iteration continues. In addition, this approach allows us to first identify the parameters or vectors that are closer to 0 with a smaller tuning parameter, resulting in a reduction in bias from the penalty terms. Once a significant penalty level is reached where redundant parameters are removed, we then gradually reduce the tuning parameters so that the bias for nonzero components can be well controlled. To implement these strategies, we introduce interval parameters Δ , expansion factors δ_1 , and shrinkage factors δ_2 . In the first half of the training process, all penalty parameters increase by a factor of δ_1 every Δ iterations. In the latter half, the parameters are decreased by a factor of δ_2 every Δ iterations. For the initial penalty parameters $\lambda_r^{(0)}, r = 1, 2, 3$, since λ_1 is used to identify the OID, while λ_2 and λ_3 are related to tuning the optimal generator architecture corresponding to the input dimension, we consider the sequential selection of $\lambda_1^{(0)}, \lambda_2^{(0)}$ and $\lambda_3^{(0)}$ via grid search in some region around zero; that is, $\lambda_1^{(0)}$ is first chosen such that λ_2 and λ_3 are fixed at 0; then, $\lambda_2^{(0)}$ is selected with λ_1 fixed at the selected value and λ_3 fixed at 0. Finally, $\lambda_3^{(0)}$ is determined with λ_1 and λ_2 fixed at the selected values.

Optimizing (11) by directly using gradient-based methods can be challenging because the penalty terms $\|\cdot\|_{1,2}$ and $\|\cdot\|_1$ are both nondifferentiable at 0. To overcome this difficulty, we employ a subgradient descent algorithm (Boyd et al., 2004) with parameter truncation. The details of subgradient can be found in Supplementary D.1. To perform parameter truncation, we introduce two additional hyperparameters, τ_1 and τ_2 , as thresholds to truncate the row $\hat{\mathbf{B}}$ with a small L_2 norm and the element $\hat{\theta}$ with a small absolute value, respectively. The value of τ_1 can be determined by identifying the point at which there is a significant decrease in the performance of the model after clipping. Following Scardapane et al. (2017), we set $\tau_2 = 0.01$ in the numerical simulation and $\tau_2 = 0.001$ in the real image datasets. Algorithm 1 presents the truncation procedure for \mathbf{B} with τ_1 . Similarly, we can obtain the truncation algorithm for θ with τ_2 .

Algorithm 1: Parameter truncation algorithm

Input: τ_1, \mathbf{B}

Output: \mathbf{B}_{trunc}

- 1 Initialization $\mathbf{B}_{trunc} \leftarrow \mathbf{B}$;
 - 2 **for** $i=1:d$ **do**
 - 3 **if** $\|\mathbf{B}_{trunc}^{[i,:]}\|_2 \leq \tau_1$ **then**
 - 4 $\mathbf{B}_{trunc}^{[i,:]} \leftarrow 0$;
 - 5 **Return** \mathbf{B}_{trunc} .
-

We iterate between updating the generator once and updating the discriminator k times (Goodfellow et al., 2014; Arjovsky et al., 2017), which are called critical steps. The entire training process is outlined in Algorithm 2.

Algorithm 2: Minibatch stochastic gradient descent training of G-GANs

Input: $\mu_n = \{X_i\}_{i=1}^n$, $\nu_m = \{Z_j\}_{j=1}^m$

Output: $\hat{\theta}$, $\hat{\mathbf{B}}$, \hat{w}

```
1 Initialization  $\theta$ ,  $\mathbf{B}$ ,  $w$ ;  
2 for number of training iterations do  
3   if interval  $\Delta$  step and in the first half of training iterations then  
4      $\lfloor$  increase the penalty parameters by a factor of  $\delta_1$ ;  
5   else if interval  $\Delta$  step then  
6      $\lfloor$  decrease the penalty parameters by a factor of  $\delta_2$ ;  
7   for k steps do  
8     Sample mini-batch of  $b$  samples  $\{Z_1, \dots, Z_b\}$  from source distribution  $\nu_m$ ;  
9     Sample mini-batch of  $b$  samples  $\{X_1, \dots, X_b\}$  from the empirical target distribution  
10     $\mu_n$ ;  
10    Update the discriminator by ascending its stochastic gradient:  
10     $\nabla_w \frac{1}{b} \sum_{i=1}^b [f_w(X_i) - f_w(g_\theta(\mathbf{B}Z_i))]$ ;  
11   Sample mini-batch of  $b$  samples  $\{Z_1, \dots, Z_b\}$  from source distribution  $\nu_m$ ;  
12   Update the generator by descending its stochastic gradient:  
12    $\nabla_{\theta, \mathbf{B}} \frac{1}{b} \sum_{i=1}^b -f_w(g_\theta(\mathbf{B}Z_i)) + \mathcal{L}_{reg}(\mathbf{B}, \theta)$ , where  
12    $\mathcal{L}_{reg}(\mathbf{B}, \theta) = \lambda_1 \|\mathbf{B}\|_{1,2} + \lambda_2 (\sum_{l=1}^{L_g-1} \|A_l - \mathbf{I}\|_1 + \|c_l\|_1) + \lambda_3 \|\theta\|_1$ ; if truncating  $\mathbf{B}$  then  
13    $\lfloor$  Truncating  $\mathbf{B}$  according to Algorithm 1;  
14 Return  $\hat{\theta}$ ,  $\hat{\mathbf{B}}$ ,  $\hat{w}$ .
```

5 Experiments

In this section, we investigate the performance of the proposed G-GANs by comparing it with the existing GANs. We evaluate the ability of G-GANs in identifying the OID and the corresponding generator network in various scenarios. This includes simulated data with diverse distributions, the CT slice dataset (Dua et al., 2019) and two benchmark datasets: MNIST (Deng, 2012) and FashionMNIST (Xiao et al., 2017).

The smoothing index β_2 of evaluation class $\mathcal{H}^{\beta_2}([0, 1]^D)$ in Theorem 2.1 is usually chosen as $\beta_2 = 1$, which induces the well-known Wasserstein distance on $[0, 1]^D$ (Villani, 2009; Huang et al., 2022) and then Wasserstein GANs (Arjovsky et al., 2017). Commonly used methods to implement Wasserstein GANs include WGAN-GP (Gulrajani et al., 2017) and SNGAN (Miyato et al., 2018). Thus, we performed our G-GANs based on WGAN-GP and SNGAN, denoted as G-GAN^W and

G-GAN^{SN}, respectively. The implementations of G-GAN^W and G-GAN^{SN} are similar to those of Algorithm 2; for additional details, please refer to Algorithm D1 and Algorithm D2 in the Supplement D.2. In addition, we also consider several variants of G-GAN^W and G-GAN^{SN} to investigate the impact of the penalties in (11). Specifically, we consider G-GAN^{W†}, G-GAN^{W‡}, G-GAN^{SN†} and G-GAN^{SN‡}, where G-GAN^{W†} and G-GAN^{SN†} solely focuses on the sparsity penalty, i.e., $\mathcal{L}_{reg}(\mathbf{B}, \theta) = \lambda_3 \|\theta\|_1$, and the G-GAN^{W‡} and G-GAN^{SN‡} simultaneously consider the selection of the input dimension and sparse structure, i. e., $\mathcal{L}_{reg}(\mathbf{B}, \theta) = \lambda_1 \|\mathbf{B}\|_{1,2} + \lambda_3 \|\theta\|_1$. For clarity and convenience, we use G-GANs[†] to denote G-GAN^{W†} and G-GAN^{SN†} and G-GANs[‡] for G-GAN^{W‡} and G-GAN^{SN‡}.

We evaluate the performance of the methods by comparing the empirical distribution $\hat{\mu}_N = \frac{1}{N} \sum_{i=1}^N \delta_{\hat{\mathbf{X}}_i}$ generated by G-GANs with the true empirical distribution $\mu_M = \frac{1}{M} \sum_{j=1}^M \delta_{\mathbf{X}_j}$ in terms of maximum mean discrepancy (MMD) (Li et al., 2015; Dziugaite et al., 2015) and the Fréchet inception distance (FID) (Heusel et al., 2017), defined as

$$\begin{aligned} \text{MMD}^2(\hat{\mu}_N, \mu_M) &= \|\mathbb{E}_{\hat{\mathbf{X}} \sim \hat{\mu}_N} \varphi(\hat{\mathbf{X}}) - \mathbb{E}_{\mathbf{X} \sim \mu_M} \varphi(\mathbf{X})\|_2^2 \\ &= \frac{1}{N^2} \sum_{i=1}^N \sum_{i'=1}^N k(\hat{\mathbf{X}}_i, \hat{\mathbf{X}}_{i'}) + \frac{1}{NM} \sum_{i=1}^N \sum_{j=1}^M k(\hat{\mathbf{X}}_i, \mathbf{X}_j) + \frac{1}{M^2} \sum_{j=1}^M \sum_{j'=1}^M k(\mathbf{X}_j, \mathbf{X}_{j'}), \\ \text{FID}(\hat{\mu}_N, \mu_M) &= \|m_{\hat{\mu}_N} - m_{\mu_M}\|_2^2 + \text{Tr}(\Sigma_{\hat{\mu}_N} + \Sigma_{\mu_M} - 2(\Sigma_{\hat{\mu}_N} \Sigma_{\mu_M})^{1/2}), \end{aligned}$$

where $\varphi(\cdot)$ is the feature function and $k(\cdot, \cdot)$ is the kernel function for calculating the inner products of $\varphi(\mathbf{X})$; $\{m_{\hat{\mu}_N}, \Sigma_{\hat{\mu}_N}\}$ and $\{m_{\mu_M}, \Sigma_{\mu_M}\}$ are the mean and covariance matrix of features extracted by the inception model (Szegedy et al., 2015) from $\{\hat{\mathbf{X}}_i\}_{i=1}^N$ and $\{\mathbf{X}_j\}_{j=1}^M$, respectively; and $\text{Tr}(\cdot)$ is the trace operator. To overcome tedious parameter adjustment, following Li et al. (2015), we use a mixture of K kernels spanning multiple ranges, i.e., $k(x, y) = \sum_{j=1}^K k_{\sigma_j}(x, y)$, and choose $\{\sigma_j\}_{j=1}^{K=3} = \{1, 5, 10\}$, where $k_{\sigma}(x, y) = \exp(-\frac{1}{2\sigma} \|x - y\|^2)$. Typically, the FID measures the dissimilarity between two images, whereas the MMD assesses the distinction between two vectors.

The optimization algorithm, initial values for networks and source distribution are the same

Table 1: Some common parameters settings for simulations and real data in implementation. (M1)-(M4) refer to four numerical simulations which are described in detail in Section 5.1. The architectures of generator and discriminator are denoted as $l \times w$, where l and w are the depth and width of network. The weight of gradient penalty applied only to the methods based on WGAN-GP.

Parameter name	(M1)-(M4)	CT Slices	MNIST & FashionMNIST
Generator architecture	4×90		3×256
Discriminator architecture	4×64		3×256
Initial input dimension	50		64
Learning rate	2×10^{-4}	2×10^{-4}	2×10^{-4}
Critical step	5	5	1
Training batch size	512	512	256
The weight of gradient penalty	10	5	10
The number of updates	20,000	20,000	50,000
Expansion factor δ_1	1.1	1.1	1.1
Shrinkage factor δ_2	0.9	0.9	0.9
Interval step Δ	100	100	250

for all methods involved in the numerical simulations and real data. In particular, we use the stochastic gradient descent algorithm Adam (Kingma and Ba, 2015) to train both the generator and the discriminator with first- and second-order momentum parameters of (0, 0.9). The generator parameters $\{A_l\}_{l=0}^{L_G}$ and \mathbf{B} are initialized by the normal distribution $\mathcal{N}(0, 0.004)$, and $\{c_l\}_{l=0}^{L_G}$ is initialized to 0, which is the same as the discriminator parameters. The source distribution is set as Gaussian. Parameters settings in the different datasets are summarized in Table 1. All computations are implemented via PyTorch (Paszke et al., 2019) and Numpy (Harris et al., 2020) in Python.

5.1 Numerical simulation

We start by generating the vector \mathbf{Z} from a 10-dimensional standard normal distribution. We obtain 10,000 training samples and 2,000 testing samples from the following four models.

(M1) Linear model. Let W be an 100×10 matrix with the elements $10(j-1)$ to $10j$ in the j th column being $[-1, -0.78, -0.56, -0.33, -0.11, 0.11, 0.33, 0.56, 0.78, 1]$, and zero for the remaining components in the j th column. We generate \mathbf{X} by $\mathbf{X} = W\mathbf{Z}$.

(M2) A two-layer rectified linear unit (ReLU) neural network model with sparse connections. Let W_1 be an 50×10 matrix where the elements (i, j) are $[-1, -0.5, 0, 0.5, 1]$ as i varies from $5(j-1)$ to $5j$, and the remaining elements in the j -th column of W_1 are all 0. Let us denote W_2 as an 100×50 matrix where nonzero values appear in rows $2j-1$ to $2j$ of column j , arranged cyclically by using the sequence $[-1, -0.78, -0.56, -0.33, -0.11, 0.11, 0.33, 0.56, 0.78, 1]$. Then, we generate \mathbf{X} by $\mathbf{X} = W_2\sigma(W_1\mathbf{Z})$, where $\sigma(\cdot)$ is the ReLU function.

(M3) Nonlinear model I. The data are generated by $\mathbf{X} = [(\mathbf{Y}[1:20]^T)^2/4, \mathbf{Y}[21:50]^T, \exp(\mathbf{Y}[51:70]^T), \sin(\mathbf{Y}[71:100]^T \times 20)]^T$, where $\mathbf{Y} = W\mathbf{Z}$ and W are defined in (M1).

(M4) nonlinear model II. The setting is similar to that of M3 except that we generated the data by $\mathbf{X} = [\sqrt{|\mathbf{Y}[1:20]^T|} - 0.1, \mathbf{Y}[21:50]^T, \log(\mathbf{Y}[51:70]^T) + 0.5, \cos(\mathbf{Y}[71:100]^T \times 20)]^T$.

For models (M1)-(M4), all the network architectures, initial values, learning rates, critical steps, training batch sizes, weights of gradient penalties, numbers of updates, training data, expansion factors δ_1 , shrinkage factors δ_2 and interval steps Δ are the same for all the methods involved and are listed in Table 1. In G-GANs, G-GANs[†] and G-GANs[‡], $\lambda_1^{(0)}$ is chosen from the range $[0.002, 0.004]$ with an increment of 0.0005, and $\lambda_2^{(0)}$ is varied within $[0.01, 0.03]$ with a step size of 0.005 and $\lambda_3^{(0)}$ is selected from the set $\{10^{-8}, 10^{-7}, 10^{-6}, 10^{-5}, 10^{-4}\}$.

We evaluate the performance of G-GANs in (M1)-(M4) via the MMD with $N = M = 2,000$. We denote the estimated input dimension by Dim. and the proportion of zero elements in the network model by Prop.0, which is calculated by $\text{card}(i : \hat{\theta}_i = 0) / \text{card}(\hat{\theta})$, where $\text{card}(\mathcal{A})$ is the cardinality of a set \mathcal{A} . We report the mean and standard deviation (SD) of all indices derived from 10 experimental runs in Table 2. It is clear that the proposed G-GANs significantly outperforms the baseline models in terms of the MMD across all four models. Furthermore, the estimated input dimension of G-GANs is approximately 10, aligning closely with the true dimension and confirming the consistency of the input dimension, as demonstrated in Theorem 3.1. By comparing

Table 2: The mean of maximum mean discrepancy (MMD), input dimension (Dim.) and proportion of zero elements in model parameters $\hat{\theta}$ (Prop.0) and the corresponding standard deviations (reported in parentheses) for (M1)-(M4). The reported MMD values have been scaled by a factor of 0.0001. The smallest MMDs, lowest input dimensions and highest portion of zero elements are highlighted in bold font.

Dataset	(M1)			(M2)		
Method	MMD(SD)	Dim.(SD)	Prop.0(SD)	MMD(SD)	Dim.(SD)	Prop.0(SD)
WGAN-GP	0.25(0.04)	50.00(0.00)	1.41(0.07)	4.20(4.40)	50.00(0.00)	1.79(0.13)
G-GAN ^{W†}	0.60(0.05)	50.00(0.00)	13.75(0.37)	5.10(0.69)	50.00(0.00)	19.51(1.10)
G-GAN ^{W‡}	0.34(0.06)	11.80(6.10)	24.88(0.43)	4.86(1.20)	10.40(4.19)	32.35(2.32)
G-GAN ^W (prop.)	0.11(0.02)	11.80(6.10)	91.06(0.10)	0.25(0.05)	10.40(4.19)	93.51(0.18)
SNGAN	1.03(0.15)	50.00(0.00)	1.50(0.03)	2.77(0.35)	50.00(0.00)	1.60(0.09)
G-GAN ^{SN†}	1.07(0.17)	50.00(0.00)	16.60(0.75)	2.68(0.34)	50.00(0.00)	18.50(1.48)
G-GAN ^{SN‡}	1.18(0.13)	11.00(4.20)	26.80(0.72)	2.67(0.46)	10.60(4.61)	24.30(4.32)
G-GAN ^{SN} (prop.)	0.14(0.01)	11.00(4.20)	92.16(0.33)	0.55(0.04)	10.60(4.61)	93.29(0.16)
Dataset	(M3)			(M4)		
Method	MMD(SD)	Dim.(SD)	Prop.0(SD)	MMD(SD)	Dim.(SD)	Prop.0(SD)
WGAN-GP	3.57(1.27)	50.00(0.00)	1.68(0.12)	1.58(0.44)	50.00(0.00)	1.50(0.07)
G-GAN ^{W†}	3.27(1.47)	50.00(0.00)	17.37(1.31)	1.89(0.34)	50.00(0.00)	15.88(0.74)
G-GAN ^{W‡}	3.16(0.57)	9.80(4.80)	31.81(1.07)	1.56(0.23)	12.10(5.92)	28.64(0.74)
G-GAN ^W (prop.)	0.38(0.07)	9.80(4.80)	90.63(0.23)	0.71(0.05)	12.10(5.92)	88.76(1.28)
SNGAN	3.01(1.48)	50.00(0.00)	1.55(0.07)	2.01(0.75)	50.00(0.00)	1.54(0.08)
G-GAN ^{SN†}	2.87(1.12)	50.00(0.00)	16.90(0.84)	1.83(0.68)	50.00(0.00)	15.80(0.90)
G-GAN ^{SN‡}	2.74(0.64)	11.40(5.22)	27.50(1.34)	1.75(0.37)	8.30(2.93)	26.10(2.31)
G-GAN ^{SN} (prop.)	0.25(0.01)	11.40(5.22)	91.99(0.83)	0.49(0.02)	8.30(2.93)	92.1(0.81)

G-GAN^{W†,‡} and G-GAN^{SN†,‡} with WGAN-GP and SNGAN, we see that the sparse penalty on the generator network does not yield substantial improvement. However, the penalization of the rows \mathbf{B} is effective at identifying the input dimension, although the improvements in MMD are not significant for G-GAN^{W‡} or G-GAN^{SN‡} compared to their baseline models. However, applying additional penalties to the network depth induces notably significant benefits across all indices. Specifically, upon examining the proportion of zero elements in network parameters for G-GANs and G-GANs[‡], reducing the depth drastically shrinks the network size since our initial generator network is wide. As a result, the MMD is reduced to approximately 1/10 to 1/2 of that of the baseline models across the four simulated datasets. This finding validates Theorem 2.1, highlighting the strong dependence of the generalization error on the network size.

5.2 The CT slice dataset

The CT slice dataset is available from the UCI machine learning repository and comprises a collection of 53,500 CT images obtained from 74 different patients, encompassing 43 males and 31 females. Each CT slice is described by two histograms in polar space, totaling 384 features. The first histogram delineates the location of bone structures in the image, with 240 features. The second histogram depicts the location of air inclusions within the body, with 144 features. The bins outside the image are marked with a value of -0.25 . We partition the CT slice dataset into a training set comprising 50,000 samples and a testing set of 3,500 samples.

To assess G-GANs across diverse input dimensions and generator architectures, we applied $G\text{-GAN}^W$, $G\text{-GAN}^{SN}$, WGAN-GP, and SNGAN to the CT slice dataset using two setups: one with an initial input dimension of 64 and a 4-layer generator (each layer having a width of 256) and another with an initial input dimension of 96 and a 5-layer generator (each layer featuring a width of 320). For ease of reference, these setups are denoted as $64 - 4 \times 256$ and $96 - 5 \times 320$, respectively. The discriminator architecture is the same across both settings, comprising 3 layers, each with a width of 192.

Common parameters persist across all methods and are outlined in Table 1. When implementing $G\text{-GAN}^W$ and $G\text{-GAN}^{SN}$, $\lambda_1^{(0)}$ is chosen from $[0.01, 0.05]$ in increments of 0.005, $\lambda_2^{(0)}$ from $[0.1, 0.3]$ in increments of 0.1 and $\lambda_3^{(0)}$ is selected in $\{10^{-8}, 10^{-7}, 10^{-6}, 10^{-5}, 10^{-4}\}$.

We calculate the MMD based on $N = M = 3500$ generated and test samples. Table 3 presents the mean and standard deviation (SD) of the MMD, input dimension (Dim.), and the proportion of zero elements (Prop.0) based on 5 experiments. As shown in Table 3, $G\text{-GAN}^W$ and $G\text{-GAN}^{SN}$ significantly outperform the baseline models WGAN-GP and SNGAN in both scenarios. In particular, $G\text{-GAN}^W$ displays enhancements of 7.8% and 26.6% relative to WGAN-GP, while $G\text{-GAN}^{SN}$ exhibits improvements of 74.3% and 74% relative to SNGAN. In addition, interestingly,

Table 3: The mean of maximum mean discrepancy (MMD), input dimension (Dim.) and proportion of zero elements in model parameters $\hat{\theta}$ (Prop.0) and the corresponding standard deviations (reported in parentheses) for CT slices dataset. The reported MMD values have been scaled by a factor of 0.0001. The architecture is identified by the initial input dimension and generator architecture, designated as $d - l \times w$, where d , l , w refer to the initial input dimension, depth and width of the generator, respectively. The smallest MMDs, lowest input dimensions and highest portion of zero elements are highlighted in bold font.

Dataset	CT slices					
Architecture	64 - 4 × 256			96 - 5 × 320		
Method	MMD(SD)	Dim.(SD)	Prop.0(SD)	MMD(SD)	Dim.(SD)	Prop.0(SD)
WGAN-GP	8.83(0.36)	64.00(0.00)	1.90(0.04)	10.95(1.52)	96.00(0.00)	2.12(0.02)
G-GAN ^W	8.14(0.04)	5.00(1.63)	59.30(0.07)	8.04(0.02)	5.40(1.02)	73.14(0.04)
SNGAN	26.70(10.90)	64.00(0.00)	2.25(0.17)	30.65(11.09)	96.00(0.00)	2.24(0.04)
G-GAN ^{SN}	7.95(0.01)	5.30(2.49)	57.99(0.35)	7.98(0.01)	4.60(0.50)	73.15(0.03)

the MMD and Dim. were nearly identical for G-GAN^W and G-GAN^{SN} across both scenarios. This finding suggests that the proposed G-GANs can achieve an optimal parameter set regardless of the initial input dimension and generator architecture. Moreover, both G-GAN^W and G-GAN^{SN} demonstrate an input dimension of approximately 5 in both setups, aligning closely with the estimated intrinsic dimension of 3.8 by [Facco et al. \(2017\)](#).

5.3 MNIST and FashionMNIST

Now, we illustrate the application of G-GANs for unsupervised image generation by using two well-known benchmark datasets: MNIST and FashionMNIST. The MNIST dataset includes grayscale images of handwritten digits from 0 to 9. FashionMNIST, an alternative to MNIST, presents a more challenging task with grayscale images displaying ten distinct classes, such as T-shirts, dresses, shoes, and bags. The MNIST and FashionMNIST training datasets consist of 60,000 images, each stored in a 28×28 pixel matrix with pixel intensities ranging from 0 to 1. For visual reference, we display real examples of images from MNIST and FashionMNIST in [Figure 2\(a\)](#) and [Figure 3\(a\)](#), respectively.

We applied the proposed G-GAN^W and G-GAN^{SN} and their baseline models, WGAN-GP and

SNGAN, to the two datasets. To satisfy the input requirement of the FNNs, we flatten each 28×28 image pixel matrix into a 784-dimensional vector. The parameter settings remain consistent across all methods and are listed in Table 1. When implementing G-GANs, $\lambda_1^{(0)}$ is chosen from $[0.001, 0.01]$ in increments of 0.001 for G-GAN^W, while $[0.0001, 0.0005]$ in increments of 0.001 for G-GAN^{SN}, $\lambda_2^{(0)}$ ranges from $[0.01, 0.03]$ in steps of 0.01 and $\lambda_3^{(0)}$ is selected in $\{10^{-8}, 10^{-7}, 10^{-6}, 10^{-5}, 10^{-4}\}$ for both methods.

The performances of the generated samples are evaluated via FID, which is calculated based on $N = M = 60,000$ generated and training samples. Table 4 reports the mean and standard deviation of the FID, the input dimension (Dim.) and the proportion of zero elements in the model parameters (Prop.0) by repeating the experiments 3 times. Clearly, both G-GAN^W and G-GAN^{SN} outperform their baseline models, WGAN-GP and SNGAN, in terms of FID. Specifically, G-GAN^W displays enhancements of 30.7% in MNIST and 30.6% in FashionMNIST relative to WGAN-GP; G-GAN^{SN} demonstrates remarkable improvements of 55.8% in MNIST and 63.2% in FashionMNIST relative to SNGAN. Furthermore, the estimated input dimension for both MNIST and FashionMNIST is approximately 8, which is consistent with the findings of Pope et al. (2020), who estimated the intrinsic dimensions of various datasets using maximum likelihood estimation (Levina and Bickel, 2004). This consistency again implies that our G-GANs are able to identify the OID. Finally, by observing a higher proportion of zero elements in G-GANs, we see that the proposed G-GANs feature simpler generator networks.

To provide a more intuitive view, we show the real images and the images generated by WGAN-GP, G-GAN^W, SNGAN and G-GAN^{SN} for MNIST and FashionMNIST in Figure 2 and 3, respectively. It is evident that the images generated by G-GAN^W and G-GAN^{SN} are much clearer than those generated by WGAN-GP and SNGAN. Particularly, when the SNGAN loses effectiveness, G-GAN^{SN} still works, as shown in (d) and (e) of Figures 2 and 3.

Now, we explore the features of the input $\hat{\mathbf{B}}z$. In Figure 4, we present the variation in the

Table 4: The mean of Fréchet inception distance (FID), input dimension (Dim.) and proportion of zero elements in model parameters $\hat{\theta}$ (Prop.0) and the corresponding standard deviations (reported in parentheses) for MNIST and FashionMNIST. The smallest FIDs, lowest input dimensions and highest portion of zero elements are highlighted in bold font.

Dataset	MNIST			FashionMNIST		
Method	FID(SD)	Dim.(SD)	Prop.0(SD)	FID(SD)	Dim.(SD)	Prop.0(SD)
WGAN-GP	144.10(51.36)	64.00(0.00)	1.31(0.27)	113.50(3.51)	64.00(0.00)	1.24(0.02)
G-GAN ^W	99.86(3.94)	7.70(0.47)	32.62(0.03)	78.65(2.01)	7.7(0.47)	33.03(0.03)
SNGAN	239.26(51.14)	64.00(0.00)	3.19(1.06)	340.00(12.77)	64.00(0.00)	3.10(0.05)
G-GAN ^{SN}	105.70(1.45)	7.70(0.47)	31.97(0.14)	125.19(2.93)	7.70(2.36)	33.23(0.08)

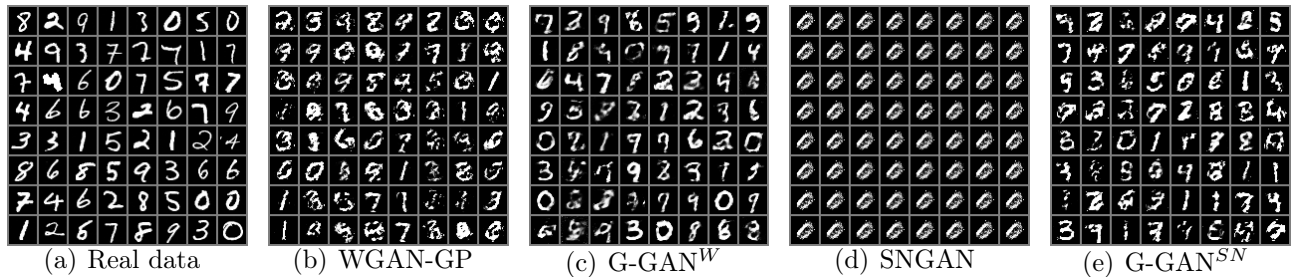


Figure 2: Observed images (a) and generated images (b) – (e) by WGAN-GP, G-GAN^W, SNGAN and G-GAN^{SN}, respectively for MNIST.

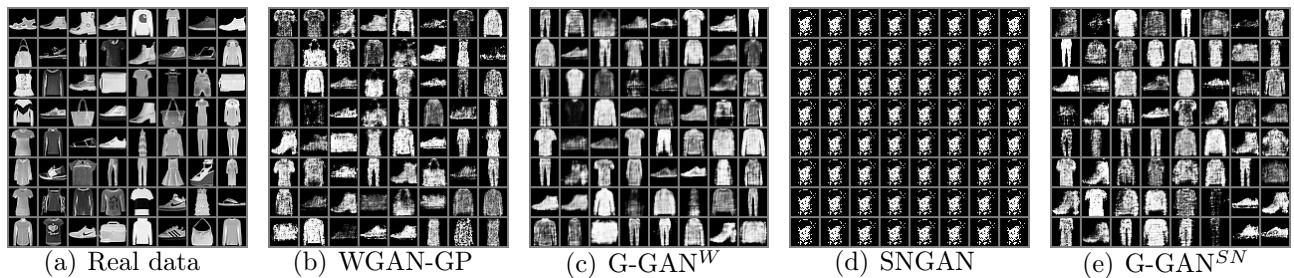


Figure 3: Observed images (a) and generated images (b)–(e) by WGAN-GP, G-GAN^W, SNGAN and G-GAN^{SN}, respectively, for FashionMNIST.

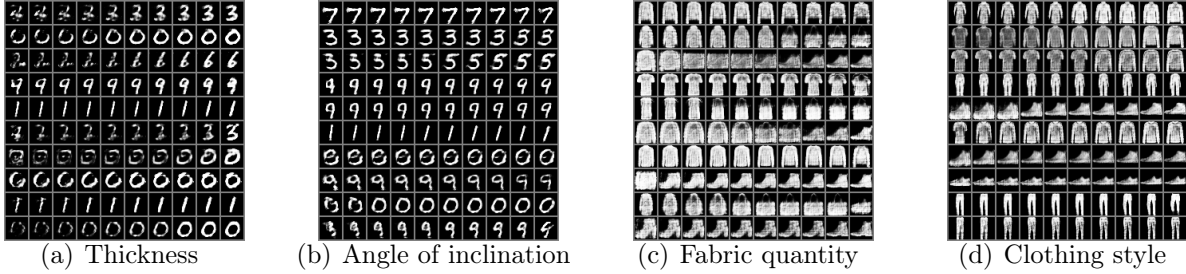


Figure 4: The manipulation of input variables in the MNIST and FashionMNIST datasets. Each block in the figures corresponds to the traversal of a single input variable while keeping the others fixed. Each row in the figures represents a different image. The traversal is conducted within the range of $[-2, 2]$. In MNIST, the selected input variables correspond to the thickness of the digit (a) and the angle of inclination of the digit (b). While in FashionMNIST, the selected input variables correspond to the fabric quantity (c) and the clothing style (d).

generated samples in MNIST and FashionMNIST as two components of the $\hat{\mathbf{B}}z$ change. Each subfigure in Figure 4 corresponds to the variation in a specific input variable while holding the others constant. Each row in the subfigures represents a different generation sample derived from the two components in $\hat{\mathbf{B}}z$ spanning from -2 to 2 . Interestingly, the two chosen input variables in MNIST corresponded to the thickness (Figure 4(a)) and the angle of inclination (Figure 4(b)) of the digits. In FashionMNIST, the two selected input variables correspond to the fabric quantity (Figure 4(c)) and the clothing style (Figure 4(d)). These results indicate that the inputs identified by $\hat{\mathbf{B}}z$ align with visually prominent features, implying that when compressed to the OID, the inputs might be interpretable. Additional experimental results regarding the interpretability of G-GAN-identified inputs for the RING, Swiss Roll, and GRID datasets (Chen et al., 2022) can be found in the Supplementary Materials E.3.

6 Conclusion

In this study, we investigate how the input dimension impacts the generalization error of GANs. In our theoretical analysis., we first explore the trade-off between the generator approximation and the statistical errors, confirming the existence of an OID that minimizes the generalization

error of the GANs. Moreover, the theoretical results imply that this reduction in dimensionality also minimizes the required size of the generator network architecture. This leads to further enhancements in the accuracy and stability of the estimation and prediction results. To determine the OID, we creatively introduce a matrix \mathbf{B} into the GANs, resulting in G-GANs. By applying a group sparse penalty to \mathbf{B} and by developing an architecture penalty for the generator g , we establish an adaptable estimation for the input dimension and the corresponding generator architecture. Rigorous theoretical evidence supports the consistency of the proposed method in terms of both the input dimension and generator architecture. Extensive numerical experiments, including on three benchmark datasets, demonstrate the superior performance of the proposed G-GANs in identifying the input dimension and generator architecture. leading to a substantial improvement in both accuracy and stability for estimation and generation. In addition, interestingly, the identified inputs align with visually significant features, such as the thickness and angle of inclination of digits in MNIST and the fabric quantity and clothing styles in FashionMNIST.

Several important research directions warrant further investigation. First, simulation studies and three benchmark datasets suggest that the optimal input dimension is close to the intrinsic dimension d^* . Providing theoretical support for this observation is of interest. Second, as illustrated in Figure 4 and supplementary Figure E3, when compressed to the OID, the variables $\mathbf{B}z$ seem to align with visually significant features. It is highly meaningful to further explore the structure of \mathbf{B} to ensure the interpretability of $\mathbf{B}z$. Third, contrary to the notion that larger generator architectures are always preferable, our theoretical and practical analysis reveals that the "bigger is better" belief does not hold true, which is consistent with the lottery ticket hypothesis (Chen et al., 2020b; Yeo et al., 2023). However, there is no theoretical guarantee for this hypothesis. Establishing theoretical evidence for the lottery ticket hypothesis through generalized error decomposition is worthwhile.

References

- Arjovsky, M. and Bottou, L. (2017). Towards principled methods for training generative adversarial networks. In *International Conference on Learning Representations*.
- Arjovsky, M., Chintala, S., and Bottou, L. (2017). Wasserstein generative adversarial networks. In *Proceedings of the 34th International Conference on Machine Learning-Volume 70*, pages 214–223. PMLR.
- Arora, S., Ge, R., Liang, Y., Ma, T., and Zhang, Y. (2017). Generalization and equilibrium in generative adversarial nets (gans). In *34th International Conference on Machine Learning*, pages 322–349. International Machine Learning Society (IMLS).
- Bailey, B. and Telgarsky, M. J. (2018). Size-noise tradeoffs in generative networks. In *Proceedings of the 32nd International Conference on Neural Information Processing Systems*, pages 6490–6500.
- Barron, A. R. (1993). Universal approximation bounds for superpositions of a sigmoidal function. *IEEE Transactions on Information theory*, 39(3):930–945.
- Bartlett, P. L., Harvey, N., Liaw, C., and Mehrabian, A. (2019). Nearly-tight vc-dimension and pseudodimension bounds for piecewise linear neural networks. *The Journal of Machine Learning Research*, 20(1):2285–2301.
- Bellido, I. (1993). Do backpropagation trained neural networks have normal weight distributions? In *ICANN’93: Proceedings of the International Conference on Artificial Neural Networks Amsterdam, The Netherlands 13–16 September 1993 3*, pages 772–775. Springer.
- Block, A., Jia, Z., Polyanskiy, Y., and Rakhlin, A. (2022). Intrinsic dimension estimation using wasserstein distance. *The Journal of Machine Learning Research*, 23(1):14124–14160.
- Bottou, L. (2010). Large-scale machine learning with stochastic gradient descent. In *Proceedings of COMPSTAT’2010: 19th International Conference on Computational Statistics Paris France, August 22-27, 2010 Keynote, Invited and Contributed Papers*, pages 177–186. Springer.
- Boyd, S., Boyd, S. P., and Vandenberghe, L. (2004). *Convex optimization*. Cambridge university press.
- Chen, M., Liao, W., Zha, H., and Zhao, T. (2020a). Distribution approximation and statistical estimation guarantees of generative adversarial networks. *arXiv preprint arXiv:2002.03938*.
- Chen, X., Zhang, Z., Sui, Y., and Chen, T. (2020b). Gans can play lottery tickets too. In *International Conference on Learning Representations*.
- Chen, Y., Gao, Q., and Wang, X. (2022). Inferential wasserstein generative adversarial networks. *Journal of the Royal Statistical Society Series B: Statistical Methodology*, 84(1):83–113.
- Colding, T. H. and Minicozzi, W. P. (2014). Lojasiewicz inequalities and applications. *Surveys in Differential Geometry*, 19(1):63–82.

- Dahal, B., Havrilla, A., Chen, M., Zhao, T., and Liao, W. (2022). On deep generative models for approximation and estimation of distributions on manifolds. *Advances in Neural Information Processing Systems*, 35:10615–10628.
- Deng, L. (2012). The mnist database of handwritten digit images for machine learning research. *IEEE Signal Processing Magazine*, 29(6):141–142.
- Dinh, V. and Ho, L. S. T. (2020a). Consistent feature selection for analytic deep neural networks. In *Proceedings of the 34th International Conference on Neural Information Processing Systems*, pages 2420–2431.
- Dinh, V. and Ho, L. S. T. (2020b). Consistent feature selection for neural networks via adaptive group lasso. *arXiv preprint arXiv:2006.00334*.
- Dua, D., Graff, C., et al. (2019). Uci machine learning repository, 2017. URL <http://archive.ics.uci.edu/ml>, 7(1).
- Dziugaite, G. K., Roy, D. M., and Ghahramani, Z. (2015). Training generative neural networks via maximum mean discrepancy optimization. In *Proceedings of the Thirty-First Conference on Uncertainty in Artificial Intelligence*, pages 258–267.
- Facco, E., d’Errico, M., Rodriguez, A., and Laio, A. (2017). Estimating the intrinsic dimension of datasets by a minimal neighborhood information. *Scientific reports*, 7(1):12140.
- Glorot, X. and Bengio, Y. (2010). Understanding the difficulty of training deep feedforward neural networks. In *Proceedings of the Thirteenth International Conference on Artificial Intelligence and Statistics, AISTATS 2010*, volume 9, pages 249–256.
- Goodfellow, I. J., Pouget-Abadie, J., Mirza, M., Xu, B., Warde-Farley, D., Ozair, S., Courville, A., and Bengio, Y. (2014). Generative adversarial nets. In *Proceedings of the 27th International Conference on Neural Information Processing Systems-Volume 2*, pages 2672–2680.
- Gulrajani, I., Ahmed, F., Arjovsky, M., Dumoulin, V., and Courville, A. (2017). Improved training of wasserstein gans. In *Proceedings of the 31st International Conference on Neural Information Processing Systems*, pages 5769–5779.
- Harris, C. R., Millman, K. J., van der Walt, S. J., Gommers, R., Virtanen, P., Cournapeau, D., Wieser, E., Taylor, J., Berg, S., Smith, N. J., Kern, R., Picus, M., Hoyer, S., van Kerkwijk, M. H., Brett, M., Haldane, A., del Río, J. F., Wiebe, M., Peterson, P., Gérard-Marchant, P., Sheppard, K., Reddy, T., Weckesser, W., Abbasi, H., Gohlke, C., and Oliphant, T. E. (2020). Array programming with NumPy. *Nature*, 585(7825):357–362.
- He, K., Zhang, X., Ren, S., and Sun, J. (2016). Deep residual learning for image recognition. In *2016 IEEE Conference on Computer Vision and Pattern Recognition (CVPR)*, volume 1, page 770. IEEE.

- Heusel, M., Ramsauer, H., Unterthiner, T., Nessler, B., and Hochreiter, S. (2017). Gans trained by a two time-scale update rule converge to a local nash equilibrium. In *Proceedings of the 31st International Conference on Neural Information Processing Systems*, pages 6629–6640.
- Huang, J., Jiao, Y., Li, Z., Liu, S., Wang, Y., and Yang, Y. (2022). An error analysis of generative adversarial networks for learning distributions. *Journal of Machine Learning Research*, 23(116):1–43.
- Huang, Z., Shao, W., Wang, X., Lin, L., and Luo, P. (2021). Rethinking the pruning criteria for convolutional neural network. *Advances in Neural Information Processing Systems*, 34:16305–16318.
- Ji, S., Kollár, J., and Shiffman, B. (1992). A global Łojasiewicz inequality for algebraic varieties. *Transactions of the American Mathematical Society*, 329(2):813–818.
- Jiao, Y., Shen, G., Lin, Y., and Huang, J. (2023). Deep nonparametric regression on approximate manifolds: Nonasymptotic error bounds with polynomial prefactors. *The Annals of Statistics*, 51(2):691–716.
- Karras, T., Laine, S., and Aila, T. (2019). A style-based generator architecture for generative adversarial networks. In *2019 IEEE/CVF Conference on Computer Vision and Pattern Recognition (CVPR)*, pages 4396–4405. IEEE Computer Society.
- Kingma, D. P. and Ba, J. (2015). Adam: A method for stochastic optimization. In *International Conference on Learning Representations*.
- Lee, H., Ge, R., Ma, T., Risteski, A., and Arora, S. (2017). On the ability of neural nets to express distributions. In *Conference on Learning Theory*, pages 1271–1296. PMLR.
- Levina, E. and Bickel, P. J. (2004). Maximum likelihood estimation of intrinsic dimension. In *Proceedings of the 17th International Conference on Neural Information Processing Systems*, pages 777–784.
- Li, Y., Swersky, K., and Zemel, R. (2015). Generative moment matching networks. In *Proceedings of the 32nd International Conference on International Conference on Machine Learning-Volume 37*, pages 1718–1727. PMLR.
- Lu, Y. and Lu, J. (2020). A universal approximation theorem of deep neural networks for expressing probability distributions. In *Proceedings of the 34th International Conference on Neural Information Processing Systems*, pages 3094–3105.
- Miyato, T., Kataoka, T., Koyama, M., and Yoshida, Y. (2018). Spectral normalization for generative adversarial networks. In *International Conference on Learning Representations*.
- Mroueh, Y., Li, C. L., Sercu, T., Raj, A., and Cheng, Y. (2018). Sobolev gan. In *International Conference on Learning Representations*.

- Müller, A. (1997). Integral probability metrics and their generating classes of functions. *Advances in Applied Probability*, 29(2):429–443.
- Nakada, R. and Imaizumi, M. (2020). Adaptive approximation and generalization of deep neural network with intrinsic dimensionality. *The Journal of Machine Learning Research*, 21(1):7018–7055.
- Paszke, A., Gross, S., Massa, F., Lerer, A., Bradbury, J., Chanan, G., Killeen, T., Lin, Z., Gimelshein, N., Antiga, L., et al. (2019). Pytorch: an imperative style, high-performance deep learning library. In *Proceedings of the 33rd International Conference on Neural Information Processing Systems*, pages 8026–8037.
- Perekrestenko, D., Müller, S., and Bölcskei, H. (2020). Constructive universal high-dimensional distribution generation through deep relu networks. In *International Conference on Machine Learning*, pages 7610–7619. PMLR.
- Pope, P., Zhu, C., Abdelkader, A., Goldblum, M., and Goldstein, T. (2020). The intrinsic dimension of images and its impact on learning. In *International Conference on Learning Representations*.
- Radford, A., Metz, L., and Chintala, S. (2016). Unsupervised representation learning with deep convolutional generative adversarial networks. In *International Conference on Learning Representations*.
- Scardapane, S., Comminiello, D., Hussain, A., and Uncini, A. (2017). Group sparse regularization for deep neural networks. *Neurocomputing*, 241:81–89.
- Schreuder, N., Brunel, V.-E., and Dalalyan, A. (2021). Statistical guarantees for generative models without domination. In *Algorithmic Learning Theory*, pages 1051–1071. PMLR.
- Shen, Z. (2020). Deep network approximation characterized by number of neurons. *Communications in Computational Physics*, 28(5):1768–1811.
- Srivastava, R. K., Greff, K., and Schmidhuber, J. (2015). Training very deep networks. In *Proceedings of the 28th International Conference on Neural Information Processing Systems-Volume 2*, pages 2377–2385.
- Szegedy, C., Jia, Y., Sermanet, P., Anguelov, D., Erhan, D., Vanhoucke, V., Liu, W., Reed, S., and Rabinovich, A. (2015). Going deeper with convolutions. In *Proceedings of the IEEE Computer Society Conference on Computer Vision and Pattern Recognition*, pages 1–9.
- Villani, C. (2009). *Optimal transport: old and new*, volume 338. Springer.
- Xiao, H., Rasul, K., and Vollgraf, R. (2017). Fashion-mnist: a novel image dataset for benchmarking machine learning algorithms. *arXiv preprint arXiv:1708.07747*.
- Yang, Y., Li, Z., and Wang, Y. (2022). On the capacity of deep generative networks for approximating distributions. *Neural Networks*, 145:144–154.

- Yarotsky, D. (2017). Error bounds for approximations with deep relu networks. *Neural Networks*, 94:103–114.
- Yarotsky, D. (2018). Optimal approximation of continuous functions by very deep relu networks. In *Conference On Learning Theory*, pages 639–649. PMLR.
- Yeo, S., Jang, Y., Sohn, J.-y., Han, D., and Yoo, J. (2023). Can we find strong lottery tickets in generative models? In *Proceedings of the AAAI Conference on Artificial Intelligence*, volume 37, pages 3267–3275.
- Yuan, M. and Lin, Y. (2006). Model selection and estimation in regression with grouped variables. *Journal of the Royal Statistical Society: Series B (Statistical Methodology)*, 68(1):49–67.
- Zhang, P., Liu, Q., Zhou, D., Xu, T., and He, X. (2018). On the discrimination-generalization tradeoff in GANs. In *International Conference on Learning Representations*.
- Zhou, X., Jiao, Y., Liu, J., and Huang, J. (2023). A deep generative approach to conditional sampling. *Journal of the American Statistical Association*, 118(543):1837–1848.